A&A 405, 903–908 (2003)
DOI: 10.1051/0004-6361:20030586


Astronomy & Astrophysics

# Photometric activity of the Seyfert galaxy Markarian 6 from *UBV* observations in 1970–2001

V. T. Doroshenko⋆

Crimean Laboratory of the Sternberg Astronomical Institute, University of Moscow, Russia; P/O Nauchny, 98409 Crimea, Ukraine
Isaac Newton Institute of Chile, Crimean Branch

Received 10 December 2002 /Accepted 21 March 2003

**Abstract.** The light curve of Mrk 6 for 1970–2002 is presented and discussed. The amplitudes of variability were $1.6^{\rm m}$, $1.1^{\rm m}$, and $0.8^{\rm m}$ in *UBV* bands, respectively. The magnitudes of the underlying galaxy in the 27.5″ aperture were found to be $U_{\rm g} = 15.82$, $B_{\rm g} = 15.42$ and $V_{\rm g} = 14.36$. The mean color indices of the variable component are $(U-B)_{\rm var} = -0.49$ and $(B-V)_{\rm var} = 0.75$ without correction for reddening. In the time intervals from 10 days to 1300 days the structure function can be presented as a power function, $SF \propto \tau^b$, where $b = 0.72 \pm 0.04$. The time where the *SF* for Mrk 6 reaches the upper plateau is about 3300 days. The observed *SF* can be interpreted by the superposition of independent flares model with the maximal duration of flares ~800 days. If these flares are located in the radiation pressure dominated region of the accretion disk, the size of this region is about 70, 330 $R_{\rm S}$, assuming the viscous parameter $\alpha$ is 0.1, 0.01, respectively. It is concluded that the optical long-term variability of Seyfert galaxies can be explained by thermal instability in the accretion disk.

**Key words.** galaxies: active – galaxies: individual: Mrk 6 – galaxies: nuclei – galaxies: Seyfert

## 1. Introduction

Among active galaxies, the Seyfert Galaxy Markarian 6 (Mrk 6, $z = 0.0187$) was one of the first that showed variability of its H$\beta$ emission line profile. The morphological type of this galaxy is S0a. The interstellar extinction is $A_V = 0.66$ (Koski 1978; Malkan & Oke 1983). Despite its proximity ($D = 77$ Mpc, $H_0 = 75$ km s$^{-1}$ Mpc$^{-1}$), brightness and variability of emission line profiles, Mrk 6 has been very poorly studied in the optical broadband. To my knowledge only three papers with more or less systematic photometric observations of Mrk 6 have been published (Doroshenko 1988; Neizvestny 1986, 1987). This is the reason why adding new photometric data is very useful for studying its variability on long and short time scales.

In this paper, I present the results of a photometric study using *UBV* and spectral observations of Mrk 6. *UBV* observations of Mrk 6 since 1986 are presented in Sect. 2. I discuss the surface brightness distribution in the object in Sect. 3. My *UBV* data combined with *UBV* data by Neizvestny (1986, 1987) and also with continuum fluxes near the H$\beta$ emission line from archive spectra 1970–1991 (Doroshenko & Sergeev 2003) are shown in Sect. 4. The color indices of variable source are given in Sect. 5. All the photometric data are analyzed using a structure function (Sect. 6) and results are discussed in Sect. 7. Section 8 summarizes the results.

⋆ e-mail: doroshen@sai.crimea.ua

## 2. Observations

I began systematic observation of this galaxy with *UBV* photometry in 1986. A photometer with a photo-multiplier detector is attached to the 60-cm Zeiss telescope at the Crimean Laboratory of the Sternberg Astronomical Institute of Moscow University. The instrumental system is close to Johnson's standard photometric system. The observations were made through the aperture $A = 27.5''$. The star with the coordinates $\alpha = 06^{\rm h}49^{\rm m}33.1^{\rm s}$, $\delta = +74°30'45''$ (2000) was taken as a comparison star. Its magnitudes obtained several times in different years are $V = 10.66 \pm 0.01$, $B = 11.18 \pm 0.01$ and $U = 11.13 \pm 0.03$. The observed *UBV* magnitudes of Mrk 6 with their uncertainties are given in Table 1[1]. Here I give several rows from Table 1. The errors quoted in Table 1 are $1\sigma$ internal errors due to photon-counting statistics. The actual scatter seems to be slightly (~10–15%) bigger than the errors I give, due to other small external errors.

## 3. The surface brightness distribution

In order to estimate the contribution of the host galaxy in *UBV* magnitudes and to compute *UBV* magnitudes of the nucleus one needs to know the surface brightness distribution (SBD). From *UBV* observations of Mrk 6 by Neizvestny (1986) through the apertures from 4.3″ to 55″ and partly from

[1] Because of size, this table is only available in electronic at http://www.edpsciences.org.

**Table 1.** The observed *UBV* magnitudes of Mrk 6 through $A = 27.5''$.

| JD 24 400 000+ | $U$ | $\sigma U$ | $B$ | $\sigma B$ | $V$ | $\sigma V$ |
|---|---|---|---|---|---|---|
| 06450.530 | 14.82 | 0.08 | 14.93 | 0.02 | 13.88 | 0.02 |
| 06467.427 | 14.94 | 0.08 | 14.88 | 0.03 | 13.94 | 0.02 |
| ... | ... | ... | ... | ... | ... | ... |
| 12349.388 | 15.19 | 0.25 | 14.89 | 0.04 | 13.90 | 0.03 |
| 12369.276 | 14.64 | 0.10 | 14.90 | 0.03 | 13.82 | 0.04 |

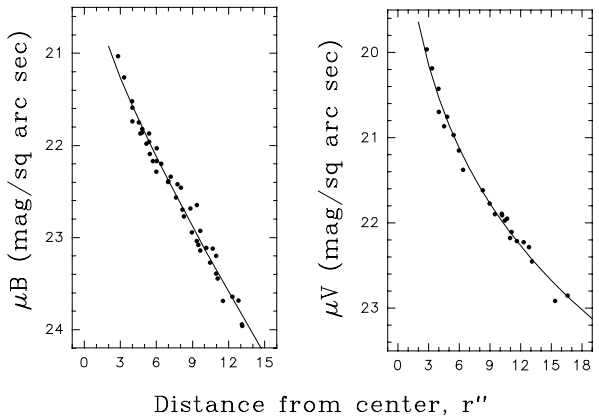


**Fig. 1.** The surface brightness distributions in $B$ and $V$ bands obtained from combined data by Neizvestny (1986) and Doroshenko (this work).

my observations through the different apertures I could obtain the surface brightness distributions (SBD) for $B$ and $V$ bands (Fig. 1). It allows one to calculate the magnitudes of the stellar component in different apertures in $B, V$. In $U$ band the SBD has quite large uncertainties. Thus I took $(U-B)_g$ from Vaucouleurs (1961) according to the morphological type S0a of Mrk 6. In such a case, the magnitudes of galaxy in $A = 27.5''$ calculated from the surface brightness distribution in $B, V$, on the one hand, and from relationship between morphological type of normal galaxies and their color indices, on the other hand, are $U_g = 15.82$, $B_g = 15.42$ and $V_g = 14.36$.

## 4. The light curves

The light curves of Mrk 6 in *UBV* bands since 1986 are shown in Fig. 2 by filled circles. The results of *UBV* observations by Neizvestny (1987) made in 1979–1984 at the 60-cm telescope of the Special Astrophysical Observatory in the Caucasus are shown by open circles. These photometric observations reveal the significant variability of the nucleus with an amplitude of about $1.6^m$, $1.1^m$ and $0.8^m$ in *UBV*-bands respectively. The ratio of the rms fluctuations to the mean flux corrected for the effect of the measurement errors is 26%, 19% and 13% in $U, B, V$ bands. As in other Seyfert galaxies the maximal variability is in the $U$-band.

The addition of spectral fluxes in continuum at $\lambda$ 5170 Å since 1970 (Doroshenko & Sergeev 2003) to the photometric

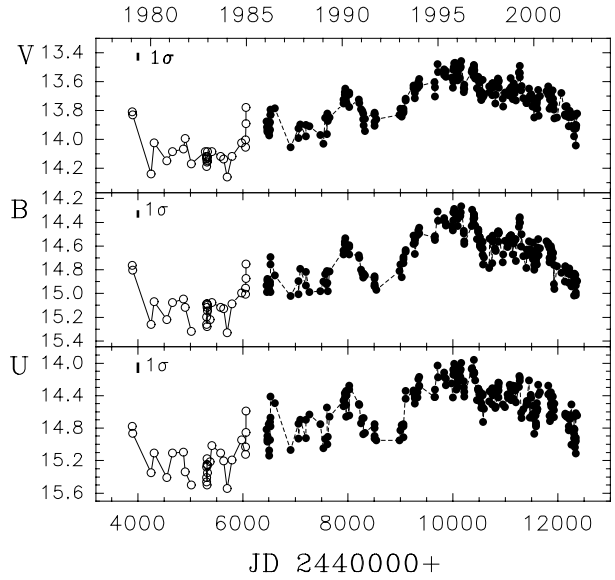


**Fig. 2.** *UBV*-light curves of Mrk 6 in $A = 27.5''$ obtained from observations by Doroshenko (filled circles) and Neizvestny (1987) (open circles).

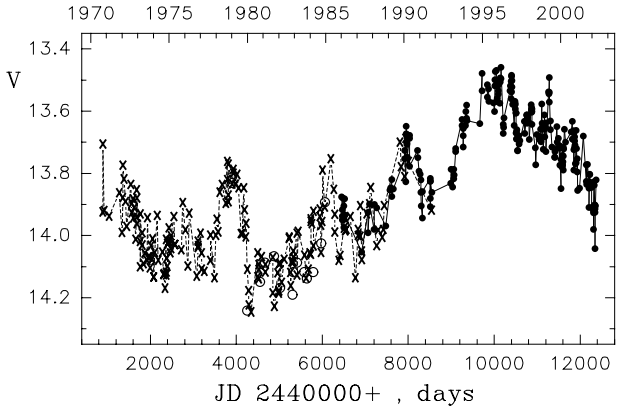


**Fig. 3.** Light curve constructed from photometric data in $V$-band by Doroshenko – filled circles, by Neizvestny (1987) – open circles and from spectral continuum flux at $\lambda$ 5170 Å by Doroshenko & Sergeev (2003) – crosses.

fluxes allows one to construct the light curve covering the period from 1970 to 2001 years. The fitting of the spectral continuum fluxes to the photometric ones was made using common dates of observations and a linear relationship between these fluxes. The combined light curve in the $V$ band is shown in Fig. 3.

The mean photometric uncertainty of the combined light curve is $0.04^m$. One can see that the full amplitude of variability in the $V$-band is $0.8^m$ and the variability is quite complicated: there are slow and fast components. The variability on the short timescale is superimposed upon the long term one.

## 5. Two-color diagram

Different physical emission mechanisms are known to produce color variations in the two-color $U-B$, $B-V$ diagram. Observed color indices of Mrk 6 before and after subtraction of the stellar

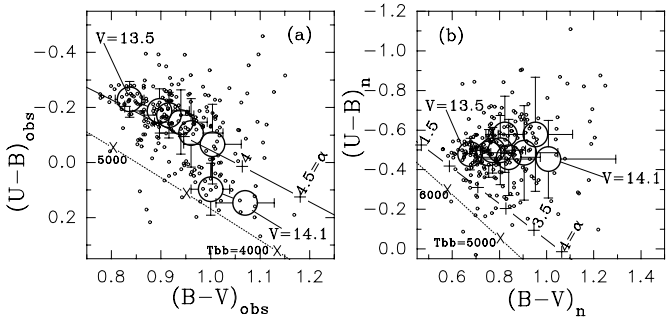


**Fig. 4.** Two-color diagram of Mrk 6 **a)** for observed values and **b)** after subtraction the underlying galaxy contribution. The colors averaged over the intervals $\Delta V = 0.1^{\rm m}$ are indicated by the large open circles. The solid line corresponds to the CI for power law spectra ($I_\nu \propto \nu^\alpha$) with different $\alpha$s; the dashed line shows the CI for black bodies with different temperature Tbb.

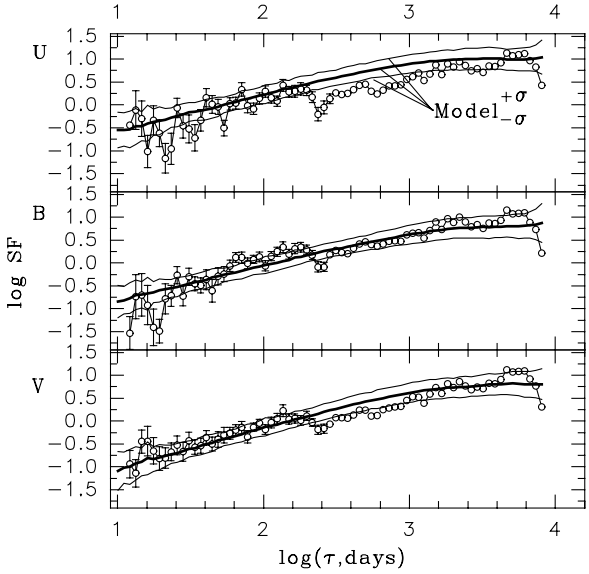


**Fig. 5.** The structure function of Mrk 6: upper panel – in *U*, middle panel – in *B* and bottom panel – in *V* band. The best fit Poisson model is shown by heavy lines. Thin lines mark the uncertainty of the *SF* ($\sigma_{SF}(\tau)$) obtained from Monte-Carlo simulations for the best fit parameters.

contribution are shown in Fig. 4. For comparison, the location of sources with power law spectra ($I_\nu \propto \nu^\alpha$) and for black body is marked in the diagrams by solid and dashed lines, respectively. The large open circles correspond to the color indices averaged over intervals $\Delta V = 0.1^{\rm m}$.

Figure 4a shows that when emission of the variable source is getting weaker (varying from $V = 13.5$ to $V = 14.1$), the color indices of the total source increase. This means that the variable component is blue and the non-variable component is redder. It is clearly seen (Fig. 4b) that the changes of color indices of the variable component have significantly less dispersion after subtraction of the underlying galaxy contribution. The weight-averaged values of the color indices for the variable sources in Mrk 6 is $(U-B)_{\rm var} = -0.49 \pm 0.02$ and $(B-V)_{\rm var} = 0.75 \pm 0.04$ without correction for reddening, $A_V = 0.66$, and $(U-B)_{\rm var} = -0.65$ and $(B-V)_{\rm var} = 0.53$ after it.

There is another way to obtain independently the color characteristics of an underlying galaxy and of a variable component, if *UBV* magnitudes of the total source are known. In such a case it is usually supposed that the variable component can only change its brightness without changing energy distribution, and the underlying galaxy is a normal galaxy. This method was successfully used by Hagen-Thorn (1985) for many active galaxies. Application of this method to the *UBV* study of Mrk 6 shows that the observed color indices of the variable component are $(U-B)_{\rm var} = -0.48 \pm 0.02$ and $(B-V)_{\rm var} = 0.58 \pm 0.02$. So, the $(U-B)_{\rm var}$ coincides very well with the estimation obtained above, but $(B-V)_{\rm var}$ is different. However, the solution obtained using the Hagen-Thorn (1985) method for the galactic component gives $(B-V)_{\rm gal} = 0.97$ and $(U-B)_{\rm gal} = 0.44$. It is in accord with the color characteristics of a S0a galaxy, if $A_V$ is about $1^{\rm m}$. Taking into account the statistical character of the relation between morphological type and color indices for normal galaxies in general, one can conclude that the agreement between the two methods is rather good.

## 6. Structure function analysis

Recently, a structure function (*SF*) analysis has been widely applied to the study of time series of active galactic nuclei (e.g. Kawaguchi et al 1998; Merkulova et al. 1999; Cid Fernandes et al. 2000; Collier & Peterson 2001; Doroshenko et al. 2001 and many others). The *SF* of the first-order is defined as

$$SF(\tau) = \left\langle [x(t) - x(t+\tau)]^2 \right\rangle,$$

where $x(t)$ is a random process, $\tau$ is time shift and angular brackets denote an ensemble average. The slope of the *SF* changes with the time interval $\tau$. On the shortest timescale, if the measurement errors are neglected, $SF \propto \tau^2$, and for long timescale *SF* converges to twice the intrinsic variance of the process: $SF \to 2\sigma^2$. The addition of photometric errors increases *SF* by the value $2\sigma^2_{\rm err}$. On intermediate timescales, i.e. $\tau_{\rm min} < \tau < \tau_{\rm max}$, the structure function is proportional to $\tau^b$ ($SF \propto \tau^b$), where the numerical value of $b$ depends on the physical mechanism responsible for the intrinsic variations. The *SF* provides estimates for both the variability time scale $\tau_{\rm min}$ and $\tau_{\rm max}$, amplitude of variability, and also the value of $b$, which is a slope of the power-law portion of the *SF*.

### 6.1. Observed and modelled SF of Mrk 6 for UBV bands

The observed *UBV SF*s of Mrk 6, corrected for the flux measurement errors, are illustrated in Fig. 5. They were computed for bins with the number of pairs available greater than 7. The error bars in Fig. 5 were calculated using multiple (400 times) realizations of flux randomization (FR) and bootstrapping (RSS) of the original data (FR/RSS method, Peterson et al. 1998).

**Table 2.** Parameters of the observed *SF*s.

| Filter | $b$ | $\sigma b$ | $r$ |
|---|---|---|---|
| **Mrk 6** | **log ($\tau$) = 1.1–2.3** | | |
| $U$ | 0.89 | 0.14 | 0.76 |
| $B$ | 1.09 | 0.07 | 0.94 |
| $V$ | 0.84 | 0.07 | 0.92 |
| $V_{p+s}$ | 1.09 | 0.11 | 0.92 |
| | **log ($\tau$) = 2.4–3.4** | | |
| $U$ | 0.83 | 0.06 | 0.94 |
| $B$ | 0.88 | 0.06 | 0.96 |
| $V$ | 0.94 | 0.05 | 0.96 |
| $V_{p+s}$ | 0.79 | 0.03 | 0.99 |
| | **log ($\tau$) = 1.1–3.4** | | |
| $U$ | 0.67 | 0.04 | 0.88 |
| $B$ | 0.74 | 0.04 | 0.91 |
| $V$ | 0.69 | 0.02 | 0.96 |
| $V_{p+s}$ | 0.79 | 0.03 | 0.98 |
| **NGC 4151** | **log ($\tau$) = 0–1.5** | | |
| **A**, *UBV* | 1.05 | 0.07 | 0.96 |
| **B**, *UBV* | 0.87 | 0.04 | 0.98 |
| | **log ($\tau$) = 1.9–3.6** | | |
| **A**, *UBV* | 0.20 | 0.04 | 0.68 |
| **B**, *UBV* | 0.75 | 0.04 | 0.98 |
| **NGC 5548** | **log ($\tau$) = 0.35–2.7** | | |
| *UBV* | 0.92 | 0.02 | 0.98 |

The observed *SF*s in different optical spectral bands are similar: all *SF*s have the first flattening located at the time shift of 210–250 days ($\log(\tau) = 2.33$–$2.37$). In the power spectrum there is a rather noticeable peak at the frequency $\nu = 0.00423$, that also corresponds to 236 days. The origin of this peak is not clear. The second flattening begins at ~3300–4000 days. The observed slopes $b$ of the *SF*s before and after the first flattening (for $\log(\tau) = 1.1$–$2.3$ and $\log(\tau) = 2.4$–$3.4$, respectively) and also the slopes in the total time interval before the upper flattening (for $\log(\tau) = 1.1$–$3.4$) are given in Table 2, where $\sigma b$ is the uncertainty of the slope, $r$ is the correlation coefficient from a linear regression, and $V_{\rm ph+spe}$ is the label for $V$ magnitudes constructed from photometric and spectral data.

The observed *SF* was compared with the *SF* for a Poisson model in which the variations of brightness were produced by the stochastic superposition of independent flares with simple Gaussian profiles randomly distributed in time. As was shown by Sergeev (1999) and also by Cid Fernandes et al. (2000), the Poisson analysis is highly insensitive to the shape of flares. According to Sergeev (1999), if the number $n$ of flares with the duration $\omega$ is given by a power law distribution, $n(\omega) \sim \omega^{\gamma}$, and if the flare amplitude, $A(\omega)$, also depends on $\omega$ as a power function, $A(\omega) \sim \omega^{\beta}$, then dependence of the *SF* on the time interval asymptotically tends to a power law shape, $SF(\tau) \sim \tau^{b}$, where $b = \gamma + 2\beta + 2$. This power law is valid when the flare duration varies between $\omega_{\rm min}$ and $\omega_{\rm max}$.

**Table 3.** The best fit model parameters for the *SF*.

| Band | $\gamma$ | $\beta$ | d$T$ | $T_{\rm min}$ | $T_{\rm max}$ | $\chi^2$ | $b$ | $\sigma b$ |
|---|---|---|---|---|---|---|---|---|
| **Mrk 6, log ($\tau$) = 1.2–3.1** | | | | | | | | |
| $U$ | –1.70 | 0.25 | 0.2 | 0.01 | 800 | 0.77 | 0.75 | 0.17 |
| $B$ | –1.59 | 0.18 | 0.2 | 0.01 | 1100 | 0.80 | 0.72 | 0.14 |
| $V$ | –1.50 | 0.20 | 0.2 | 0.01 | 900 | 0.38 | 0.82 | 0.13 |
| $V_{p+s}$ | –1.50 | 0.25 | 0.2 | 0.01 | 1000 | 0.87 | 0.90 | 0.12 |
| **NGC 4151, log ($\tau$) = –0.05–1.3** | | | | | | | | |
| $U$, **A** | –1.47 | 0.45 | 0.10 | 0.01 | 20 | 0.76 | 1.36 | 0.17 |
| **NGC 4151, log ($\tau$) = 0.03–3.0** | | | | | | | | |
| $B$, **B** | –1.70 | 0.25 | 0.25 | 0.01 | 800 | 0.77 | 0.74 | 0.06 |
| $V$, **B** | –1.60 | 0.17 | 0.20 | 0.01 | 800 | 0.64 | 0.72 | 0.06 |
| **NGC 5548, log ($\tau$) = 0.35–2.65** | | | | | | | | |
| $V$ | –1.65 | 0.32 | 0.01 | 0.001 | 250 | 1.90 | 0.92 | 0.08 |

Using Sergeev's software (1999), I have performed Monte-Carlo simulations with the following parameters: $\gamma, \beta$, and d$T$ which is the mean time interval between two sequential flares, $T_{\rm min}$ and $T_{\rm max}$ are equal to the minimal and maximal duration of flares. Unfortunately, it is impossible to obtain separately the values of the $\gamma$ and $\beta$ parameters. However, it is possible to put some restrictions on the values of $\gamma$ and $\beta$ using rational assumptions based on physical considerations and common sense. For example, one can suppose that a larger number of flares have lower amplitudes and shorter duration ($\omega$). So, $\beta$ must be larger, but $\gamma$ must be less than 0. From numerous values of $\gamma$ and $\beta$ that satisfy these conditions, we must take such values which will agree with the equation: $b = \gamma + 2\beta + 2$, where $b$ is a slope determined from the *SF*. Note, that $T_{\rm max}$ of flares cannot be more than the time corresponding to the beginning of the upper plateau in the observed *SF*. Changing these parameters, one could perform a series of Monte-Carlo light curve simulations. For each simulated light curve, the *SF* was computed in the same manner as was done for the observed light curve. The model *SF* is then given by the mean of the N simulated *SF*s, $\overline{SF(\tau)_{\rm sim}}$. The model error is given by the rms spread of the simulated model population around the mean value at each time interval $\tau$,– $\sigma_{SF}(\tau)_{\rm sim}$. The quality of the model representation of the observed *SF*s is estimated with a $\chi^2_{\rm test}$, which is calculated: $\chi^2_{\rm test} = \sum_{T_{\rm min}}^{T_{\rm max}} \frac{\left[\overline{SF(\tau)_{\rm sim}} - SF(\tau)_{\rm obs}\right]^2}{\sigma^2_{SF}(\tau)_{\rm sim}}$. The best fit parameters of the model are those for which the minimal value of $\chi^2_{\rm test}$ is obtained. These parameters are given in Table 3. In the first column of Table 2 and Table 3 $V_{p+s}$ for Mkn 6 is the combined light curve from photoelectric and spectral data.

The computed model *SF*s are also shown in Fig. 5 by heavy lines. Thin lines in Fig. 5 mark the rms of the *SF* computed from Monte-Carlo simulations for the best fit parameters. It seems that the resemblance between observations and the models is quite satisfactory.

The *SF* analysis shows that the power law portion of the *SF* delineates the range of timescales for which the variations are correlated. In order to facilitate comparison of the *SF*s in different spectral bands the *SF*s can be normalized to the value

of $\sigma^2$. So, for Mrk 6 in the *UBV* bands, normalized *SF*s on a logarithmic scale show a linear part in the interval from ~10 to ~1300 days and a mean slope $b = 0.72 \pm 0.04$. The maximal time, when the *SF* reaches the upper plateau, can be interpreted as the maximum time of correlated behaviour of points in the light curve. In practice this time is defined rather roughly and for Mrk 6 it is about 1300–3300 days. The full width of the autocorrelation function at a zero correlation level is also equal to 3900 days, in agreement with the time shift, where the upper plateau of *SF* begins. The modelling light curves in the frame of such a simple Poisson model shows that it can quite well reproduce the observed shape of the Mrk 6 light curves with the probability of about a tenth of a percent.

### 6.2. Comparison with SFs of NGC 4151 and NGC 5548

The *SF* of Mrk 6 was compared with *UBV SF*s of NGC 4151 (Czerny et al. 2003) and NGC 5548 (Doroshenko et al. 2001).

Lyuty (Lyuty & Doroshenko 1999) suggested to divide the light curve of NGC 4151 into two cycles of variability: before the deep minimum of brightness in 1989 – (Cycle A) and after that time – (Cycle B). The *UBV SF*s of NGC 4151 are noticeably different for these two periods of observations. The slopes are different for each cycle. This difference is particularly well seen in Fig. 6 and Table 2, where in the first column label **A** means Cycle A, and label **B** – Cycle B. It is possible that the difference *SF*s between Cycle A and B is caused by the increasing number of flares with larger amplitude and longer duration in Cycle B than in Cycle A.

The data from the AGNW-site by Internet[2] for NGC 5548 were added to the data in *V* band from Doroshenko et al. (2001) and the Poisson model was calculated for the combined data. Thus, the parameters for the *SF* of NGC 5548 were defined more exactly than in the earlier paper by Doroshenko et al. (2001). The *SF*s for NGC 5548 can be described by a single slope in all bands.

The plateau of the *SF*s for NGC 4151 in Cycle B begins at the time of about $\log(\tau) = 3.2{-}3.6$, whereas for NGC 5548 it begins earlier, at $\log(\tau) \approx 2.7$.

For Mrk 6 the slopes of the *SF*s in all bands are similar within the error limits, and equal to $b \sim 0.7{-}0.8$, although there is a slight flattening at time $\log(\tau) \approx 2.35$. As is noted above, the time over which the variations of brightness in Mrk 6 are not correlated (upper plateau in the *SF*) is about 1300–3300 days.

Thus the observed *SF*s for these three SyGs have some differences both in the slope *b* and in the time when the upper plateau is reached. This time is maximal for Mrk 6 and minimal for NGC 4151 in Cycle A. Moreover, the observed *SF*s of some galaxies in differing epochs of observations can change (e.g. NGC 4151). The difference in the *SF*s for these three galaxies is more clearly illustrated in Fig. 6. As one can see from the fitting of observed *SF*s by the Poisson model (see Table 3), this difference can be connected with appearing and disappearing of the longest flares in the variable component of the galaxies.

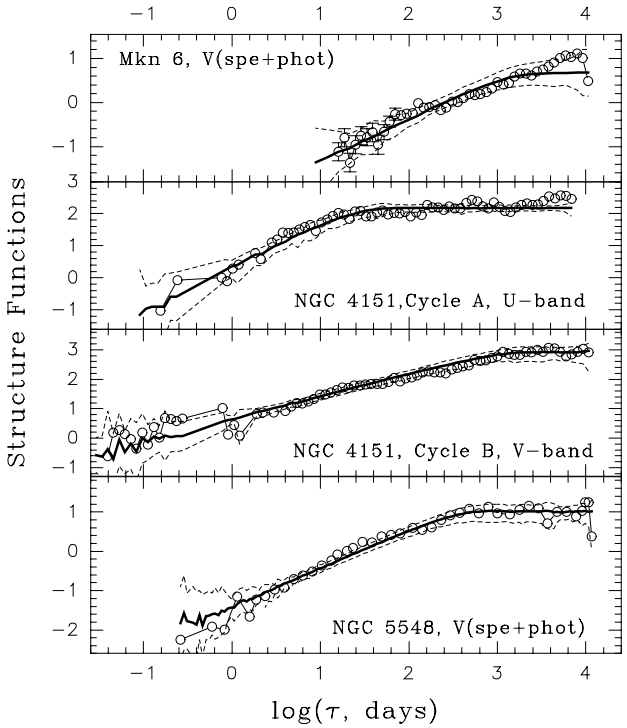


**Fig. 6.** Comparison of the *SF*s for Mrk 6, NGC 4151 and NGC 5548. The observed *SF*s are shown by open circles. The best fit Poisson models are shown by heavy lines. Dashed-lines indicate uncertainty of the model *SF*s calculated from Monte-Carlo light curve simulations. The best fit parameters of the models are given in Table 3.

## 7. Discussion

The most attractive aspect of the Poisson model is its generality. This model can include such different scenarios of the SyGs variability as accretion disk instability and starburst models. In disk instability models $T_{\max}$ can be related to the size of the active zone in the accretion disk. In starburst models this time can be connected to explosions of supernovae (SN) and the time of SN remnant evolution. But the time derived from the beginning of the upper plateau in the observed *SF*s is larger than $T_{\max}$ of the flare determined from the fitted Poisson models. This can be because by that the time of the beginning of the upper plateau in the observed *SF* includes the far wings of all previous flares, and it ought to use $T_{\max}$ derived from model fitting.

Indeed, in disk instability models the cold disk variability can be related to the thermal timescale, $t_{\rm th}$, which depends on assumptions about the properties of the accretion disk. In the classical theory of accretion disks this timescale is connected to the mass of a black hole $M_{\rm bh}$, with the distance of the emission region from the center, $r$, and with the standard disk viscosity parameter $\alpha$. In practice, I used the formula from Collier & Peterson (2001):

$$t_{\rm th} = 5.3 \left(\frac{\alpha}{0.01}\right)^{-1} \left(\frac{M_{\rm bh}}{10^7\ M_\odot}\right) \left(\frac{r}{10\ R_{\rm S}}\right)^{3/2} \text{days},$$

where $R_{\rm S}$ is the Schwarzschild's radius.

[2] http://www.astronomy.ohio-state.edu/~agnwatch/data.html.

Supposing that this time is associated with $T_{\max}$ of flares, one can estimate the size of the unstable zone of accretion disk $r$ and compare it with the radius where there is the onset of the instability, i.e. with the extension of the radiation pressure dominated zone.

The black hole mass for Mrk 6 can be estimated through the "reverberation" mass method (Wandel et al., 1999). According to the spectral study of Mrk 6 by Sergeev et al. (1999), the H$\beta$ emission line width $FWHM$ is 5540 km s$^{-1}$ and the time delay is about 18 days. Then $M_{\rm rev} = 8 \times 10^7\ M_\odot$. If the thermal timescale ($t_{\rm th}$) is assumed to be equal to $T_{\max}$ = 800 days, according to the best fit Poisson model for Mrk 6, then $(r/10\,R_{\rm S})^{3/2} = 18.9 \cdot (\alpha/0.01)$. The real value of the viscosity parameter $\alpha$ is not known. Accepting $\alpha = 0.1$ and 0.01 we obtain the estimations for the size of the unstable zone in an accretion disk $r$ from $330\,R_{\rm S}$ to $70\,R_{\rm S}$, respectively. In any case, we get quite reasonable values for the size of the thermally unstable accretion disk.

Indeed, the simple estimation of the radiation pressure dominated zone for a thin accretion disk was given by Shakura & Sunyaev (1973). More accurate descriptions of the disk vertical structure according to the calculation made by Czerny et al. (1999) has shown that the instability can start at $\sim 200\,R_{\rm S}$, and at $150\,R_{\rm S}$ the entire disk become thermally unstable. So, the thermal instability of the accretion disk is capable of explaining the long-term optical variability.

## 8. Summary

The photometric study of Mrk 6 from 1970–2001 has shown that:

- As for many Seyfert galaxies, the light curve of Mrk 6 has two components of variability: slow (months and years) and fast (days). The light curves of Mrk 6 show significant variations with amplitudes $1.6^{\rm m}$, $1.1^{\rm m}$ and $0.8^{\rm m}$ in $U, B, V$ bands, respectively. The ratio of the rms fluctuations to the mean flux corrected for measurement errors is 26%, 19% and 13% in $U, B, V$ bands.
- The slow variable component has mean observed color indices $(U-B)_{\rm var} = -0.49 \pm 0.02$ and $(B-V)_{\rm var} = 0.75 \pm 0.04$.
- The underlying galaxy has the color index of a normal S0a galaxy. Its magnitudes in the 27.5″ aperture are $U_{\rm g} = 15.82$, $B_{\rm g} = 15.42$ and $V_{\rm g} = 14.36$.
- The structure function analysis of $UBV$ light curves in Mrk 6 has shown that in the time intervals from 10 to 1300 days the $SF$ has a power law shape, $SF \propto \tau^b$, where $b = 0.72 \pm 0.04$. The time for which the variations of brightness are not correlated, i.e. when the $SF$ reaches the upper plateau, is about 3300 days.
- The observed $SF$ can be interpreted in the frame of a Poisson model in which the light variations are due to the stochastic superposition of independent flares randomly distributed in time. The maximal duration of flares in the Mrk 6 is about 800–1000 days.
- The comparison of the $SF$s of Mrk 6, NGC 4151 and NGC 5548 have shown that the time of the beginning of the upper plateau in the $SF$s varies not only from one object to other, but it can change for the same object in different periods of observation. This time is maximal for Mrk 6 and minimal for NGC 4151 in Cycle A. The striking differences between $SF$s can be connected to the appearance and disappearance the longest flares in the specific period of nuclear activity.
- Interpreting the optical variability of Mrk 6 as random flares in the radiation pressure dominated region, one can obtain the size of this region to be about $70$–$330\,R_{\rm S}$, if the viscous parameter $\alpha$ is assumed to be from 0.01 to 0.1, respectively. So, the thermal instability of the accretion disk can explain the optical long-term variability of Seyfert galaxies.

*Acknowledgements.* I would like to thank Dr. Sergeev for his permission to use the program package for data analysis. This research is supported by the grant RBRF (Russian Foundation for Basic Research) No. 00-12-16272.

## References

Cid Fernandes, R., Sodre, L. Jr., & Vieira da Silva, L. Jr. 2000, ApJ, 544, 123
Collier, S., & Peterson, B. M. 2001, ApJ, 555, 775
Czerny, B., Schwarzenberg-Czerny, A., & Loska, Z. 1999 MNRAS, 303, 148
Czerny, B., Doroshenko, V. T., Nikołajuk, M., et al. 2003, MNRAS, accepted
Doroshenko, V. T. 1988, Astrofizika, 28, 5
Doroshenko, V. T., Lyuty, V. M., Bochkarev, N. G., et al. 2001, Astron. Lett., 27, 691
Doroshenko, V. T., & Sergeev, S. G. 2003, A&A, 405, 909
Hagen-Thorn, V. A. 1985, Astrofizika, 22, 449
Kawaguchi, T., Mineshige, S., Umemura, M., et al. 1998, ApJ, 504, 671
Koski, A. T. 1978, ApJ, 223, 56
Lyuty, V. M., & Doroshenko, V. T. 1999, Astron. Lett., 25, 341
Malkan, M. A., & Oke, J. B. 1983, ApJ, 256, 92
Merkulova, N. I., Metik, L. P., & Pronik, I. I. 1999, AJ, 117, 2177
Neizvestny, S. I. 1986, Communication SAO, N51, 5
Neizvestny, S. I. 1987, Izvestia SAO, 24, 3
Peterson, B. M. Wanders, I., Horne, K., et al. 1998, PASP, 110, 660
Sergeev, S. G. 1999, Ph.D. Thesis, Crimean Astrophys. Obs.
Sergeev, S. G., Pronik, V. I., & Sergeeva, E. A., et al. 1999, ApJS, 121, 159
Shakura, N. I., & Sunyaev, R. A. 1973 A&A, 24, 337
Vaucouleurs, G., de 1961, ApJS, 5, 233
Wandel, A., Peterson, B. M., & Malkan, M. A. 1999, ApJ, 526, 579